JGR Solid Earth

RESEARCH ARTICLE
10.1029/2021JB023440

Water Enhancement of Si Self-Diffusion in Wadsleyite

Dmitry Druzhbin[1,2], Hongzhan Fei[1], Jialong Hao[3], Chi Zhang[3], Yangting Lin[3], Ralf Dohmen[4], and Tomoo Katsura[1,5]

HPSTAR 1412-2022

[1]Bayerisches Geoinstitut, University of Bayreuth, Bayreuth, Germany, [2]European Synchrotron Radiation Facility (ESRF), Grenoble, France, [3]Institute of Geology and Geophysics, Chinese Academy of Sciences, Beijing, China, [4]Institute of Geology, Mineralogy and Geophysics, Ruhr-Universität Bochum, Bochum, Germany, [5]Center for High Pressure Science and Technology Advanced Research, Beijing, China

Abstract We investigated the H_2O-content dependence of Si self-diffusion coefficient in Fe-free wadsleyite using multi-anvil experiments at pressures of 19–20 GPa, temperatures of 1573–1873 K, and H_2O-content ranging from ~10 to 5,300 wt. ppm by the isotopic thin-film diffusion-couple method. The ^{29}Si-doped diffusion profiles were measured by nanoscale secondary ion mass spectrometry in the depth profiling mode. The H_2O contents in the samples were analyzed by Fourier transformation infrared spectroscopy. The experimental results show a H_2O enhancement of Si diffusion coefficient with a H_2O content exponent of 0.8 ± 0.1. The activation enthalpy was found to be 270 ± 40 kJ/mol. The diffusion coefficients in the [100], [010], and [001] directions are indistinguishable. The temperature and H_2O-content dependences of Si diffusion indicate that H_2O incorporation dramatically reduces the rheological strength of wadsleyite, whereas temperature has a relatively small effect. The viscosity in the mantle transition zone could be significantly reduced by H_2O incorporation in wadsleyite. The viscosity contrast between mantle plumes and surroundings may control the evolution of plume shapes at 410–660 km depths.

Plain Language Summary Water incorporation in nominally anhydrous minerals may dramatically affect their physical and chemical properties by introducing additional point defects as hydroxyl in the crystal structures. In particular, the atomic diffusivity in minerals, which is controlled by the concentrations of point defects, could be enhanced, therefore, the diffusion-controlled properties such as rheology could be affected by water incorporation. Because the mantle transition zone is considered to be water-rich, we investigated the effect of water on silicon self-diffusion rate in wadsleyite, which is the dominant mineral in the upper part of mantle transition zone at 410–520 km depth. The experimental results show that water-rich (1.0 wt.% H_2O) wadsleyite is rheologically more than 2.4 orders of magnitude weaker than water-poor (less than 10 wt. ppm) conditions. Therefore, the mantle transition zone is significantly weakened by water incorporation. The viscosity contrast between plumes and surrounding mantle may control the evolution of plume shapes at mantle transition zone depths.

Key Points:

- Silicon self-diffusion in wadsleyite is enhanced by water incorporation with an exponent of 0.8 ± 0.1
- Silicon self-diffusion in wadsleyite is nearly isotropic, and has an activation energy of 270 ± 40 kJ/mol
- Viscosity contrast between plume and surrounding mantle is controlled by water and temperature, which may affect the plume shape evolution

Correspondence to:
H. Fei,
Hongzhan.fei@uni-bayreuth.de

Citation:
Druzhbin, D., Fei, H., Hao, J., Zhang, C., Lin, Y., Dohmen, R., & Katsura, T. (2022). Water enhancement of Si self-diffusion in wadsleyite. *Journal of Geophysical Research: Solid Earth*, *127*, e2021JB023440. https://doi.org/10.1029/2021JB023440

Received 18 OCT 2021
Accepted 24 FEB 2022

Author Contributions:
Conceptualization: Dmitry Druzhbin, Hongzhan Fei, Tomoo Katsura
Data curation: Dmitry Druzhbin, Hongzhan Fei
Formal analysis: Dmitry Druzhbin, Jialong Hao, Chi Zhang, Yangting Lin, Ralf Dohmen
Funding acquisition: Tomoo Katsura
Investigation: Dmitry Druzhbin, Jialong Hao, Chi Zhang, Yangting Lin, Ralf Dohmen
Methodology: Dmitry Druzhbin, Tomoo Katsura
Supervision: Hongzhan Fei, Tomoo Katsura
Validation: Dmitry Druzhbin
Visualization: Dmitry Druzhbin, Hongzhan Fei
Writing – original draft: Hongzhan Fei
Writing – review & editing: Hongzhan Fei, Tomoo Katsura

1. Introduction

The mantle transition zone located at 410–660 km depth plays a critical role in geodynamics and geochemical evolutions of the mantle. For example, the subducted slabs could stagnate at the bottom of the transition zone (Fukao et al., 2009), preventing the material transportation from the Earth's surface to the deep mantle. Dehydration melting layers can be produced at the 410 and 660-km discontinuities (Revenaugh & Sipkin, 1994; Schmandt et al., 2014). Shallow-originated hotspots can be formed in the mantle transition zone (Kuritani et al., 2019). Moreover, the plume shapes could be controlled by the viscosity contrast between the upwelling flows and the surrounding mantle (Condie, 2016).

A vital feature of the mantle transition zone is that its dominant minerals, wadsleyite and ringwoodite, can dissolve more than 1 wt.% H_2O in their crystal structures as hydroxyl (e.g., Demouchy et al., 2005; Druzhbin et al., 2021; Fei & Katsura, 2020a, 2021; Kohlstedt et al., 1996; Litasov et al., 2011; Sun et al., 2018). Therefore, the transition zone is expected to be H_2O-enriched in contrast to the relatively dry upper and lower mantle, as demonstrated by the H_2O-rich ringwoodite inclusion (Pearson et al., 2014), mineral viscosity (Fei et al., 2017), and electrical conductivity analysis (e.g., Dai & Karato, 2009; Huang et al., 2005; Karato, 2011; Kelbert et al., 2009; Manthilake et al., 2009). Because H_2O incorporation may affect the rheological properties of minerals (e.g., Costa & Chakraborty, 2008; Fei et al., 2017, 2013; Hustoft et al., 2013; Kohlstedt, 2006; Shimojuku et al., 2010),

understanding the role of H_2O on the rheology of wadsleyite and ringwoodite is essential for investigating of geodynamics in the deep mantle.

The most direct approach to understand the mineral rheology in the Earth's mantle is deformation experiments. However, sample dehydration in the open system makes it difficult to control the H_2O contents in a deformation experiment under high-pressure and high-temperature conditions. Hence, investigating the effect of H_2O on the rheological properties is challenging. The majority of the deformation studies on wadsleyite and ringwoodite were thus performed by experiments under nominally dry conditions (e.g., Farla et al., 2015; Kawazoe et al., 2010, 2011, 2013, 2016; Nishihara, Tinker et al., 2008) and by numerical modeling (e.g., Ritterbex et al., 2015, 2020). Although Hustoft et al. (2013) observed H_2O weakening of wadsleyite and ringwoodite by deformation experiments, the H_2O contents in the samples were not well controlled, as they pointed out. Thus, the H_2O effect has not been determined quantitatively.

Due to the difficulty of deformation experiments under hydrous conditions, a rather indirect method was adopted in Fei et al. (2017), that is, the H_2O effect on dislocation mobility in ringwoodite was determined based on dislocation recovery experiments, in which the samples were embedded in a closed system and therefore the H_2O contents were well controlled. By this technique, a H_2O content exponent of 1.1 ± 0.1 was obtained for the dislocation mobility in ringwoodite. Namely, H_2O has a large effect on the rheology of ringwoodite.

For wadsleyite, Shimojuku et al. (2004, 2009, 2010) adopted another indirect method. They determined the Si self-diffusion coefficients in samples with various H_2O contents by means of the isotope diffusion couple method using secondary ion mass spectroscopy (SIMS). They found that the diffusion coefficients in the samples with 10–140 wt. ppm H_2O (350–500 wt. ppm before diffusion experiments) are about half an order of magnitude higher than those with 20–60 wt. ppm H_2O (20–40 wt. ppm before diffusion), indicating a H_2O weakening of wadsleyite because the creep rate of silicate minerals is controlled by diffusion of the slowest species, which is Si in wadsleyite (Kubo et al., 2004; Shimojuku et al., 2004, 2009, 2010; Zhang et al., 2021). Nevertheless, because of the limited range of H_2O content in Shimojuku et al. (2004, 2009, 2010), they could not obtain a H_2O content exponent. Thus, the magnitude of H_2O effect on wadsleyite rheology is still unknown. Additionally, their diffusion coefficients (Shimojuku et al., 2004, 2009, 2010) were obtained from polycrystalline samples, which does not allow to identify diffusion anisotropy. The polycrystalline may also enlarge the sample surface roughness (Mullins, 1958), which in turn affects the depth resolution of the SIMS profiles (e.g., Dohmen, Becker, et al., 2002; Fei et al., 2012, 2013, 2014).

In this study, we systematically measured the Si self-diffusion coefficients in wadsleyite single crystals as a function of H_2O content from 10 to 5,300 wt. ppm at pressures of 19–20 GPa and temperatures of 1573–1873 K along the [100], [010], and [001] crystallographic axes. To reduce the surface roughness effect in SIMS analysis, the diffusion profiles were measured using a nanoscale SIMS (NanoSIMS), by which more smooth area can be analyzed by reducing the crater sizes.

2. Experimental and Analytical Procedures

2.1. Synthesis of Wadsleyite Single Crystals

Fe-free wadsleyite single crystals were synthesized at high-pressure and high temperature conditions by multi-anvil experiments using Mg_2SiO_4 forsterite powder ground from a single crystal of forsterite (Oxide Co., Japan). The impurities of the single crystal were ~80 and 82 wt. ppm of Ir and Fe, respectively, as described in Fei et al. (2012). The forsterite powder was sealed in platinum capsules with inner and outer diameters of 1.6 and 2.0 mm, respectively, by arc-welding. The adhesive moisture in the powder acted as the H_2O source. Each capsule was placed into an MgO sleeve in a $LaCrO_3$ heater with a ZrO_2 thermal insulator. A Cr_2O_3-doped MgO octahedron with edge lengths of 18 mm was used as the pressure medium (18/8 standard assembly at Bayerisches Geoinstitut, University of Bayreuth). The assembly was compressed to 21 GPa by eight pieces of tungsten carbide anvils with 8-mm truncation edge lengths, followed by annealing at a temperature of 2050 K for 2–5 hr monitored by a W/Re (D-type) thermocouple. Afterwards, the assembly was quenched to room temperature by switching off the heating power, and decompressed to ambient pressure for more than 15 hr. Finally, inclusion- and crack-free wadsleyite single crystals with 100–1,000 μm grain sizes were picked up from the sample capsules.

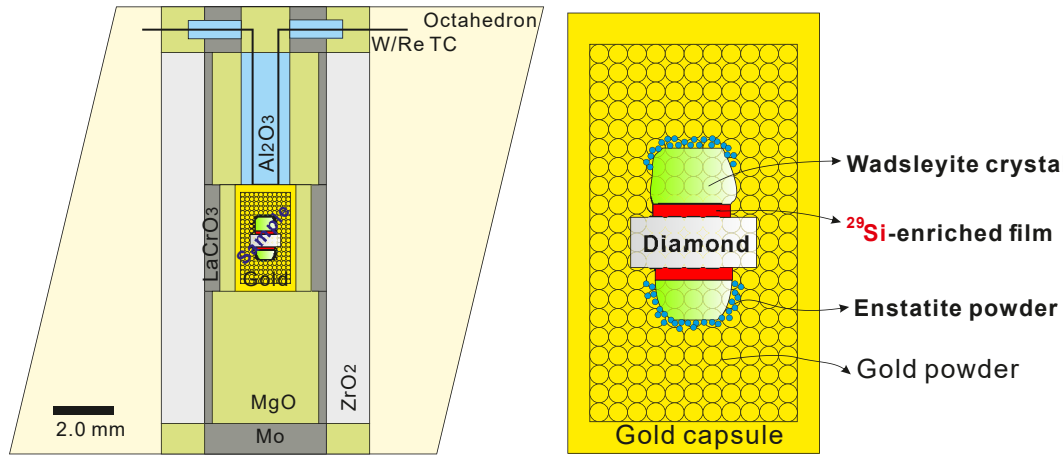

Figure 1. 18/8 multi-anvil cell assembly (left) and capsule design (right) used for diffusion experiments in this study. The thin-film coated wadsleyite single crystals faced to a diamond single crystal were embedded in gold powder within the gold capsule. The same cell assembly design but with forsterite powder within a platinum capsule was used for sample synthesis experiments.

2.2. Diffusion Experiments

The wadsleyite single crystals were oriented along the [100], [010], and [001] crystallographic axes using a single-crystal X-ray diffractometer. They were mechanically polished on the crystallographic planes using diamond powder until no scratches were recognized, and then chemically polished using an alkaline colloidal silica solution for 2–7 hr. Finally, the surface topography (hereafter defined as one standard deviation of the surface topography) was less than 3 nm. The polished surfaces were deposited with an amorphous film of 500–1,000 nm thickness produced by pulsed laser ablation on a ^{29}Si-enriched Mg_2SiO_4 target using the pulsed laser deposition system at the Ruhr-University Bochum (Dohmen, Chakraborty, et al., 2002).

To protect the thin film from mechanical damage during compression, the thin-film-coated surfaces were faced on a diamond single crystal (Figure 1), which had a topography of less than 5 nm. The thin-film-coated wadsleyite sample with the diamond crystal, together with enstatite powder at the back side of the sample to buffer the SiO_2 activity, were embedded in gold powder and welded in a gold capsule with a 2.0-mm outer diameter and 1.6-mm inner diameter. The capsule was loaded into the same cell assembly as that for the single-crystal synthesis (Figure 1), and annealed at 19–20 GPa and 1573–1873 K for 0–600 min.

2.3. Diffusion Profile Analysis

The diffusion profiles were measured using Cameca NanoSIMS 50 L installed at the Institute of Geology and Geophysics, Chinese Academy of Sciences, Beijing. A primary beam of 100 pA Cs^+ were used to scan the 10×10 μm^2 area to acquire the ion image of ^{28}Si and ^{29}Si in multi-collection mode. To avoid the edge effect from the SIMS craters, only the ^{28}Si and ^{29}Si intensity data from the central region of each crater with 2.5×2.5 μm^2 area were used to calculate the diffusion profiles (Figure 2).

The intensities of ^{29}Si and ^{28}Si were obtained as a function of sputtering time by the NanoSIMS. The depth of each SIMS crater was subsequently determined by a 3D-Nanofocus microscope at the University of Bayreuth. The time data in the SIMS analysis was converted to depth by assuming a constant sputtering rate for each crater. The ^{29}Si/(^{29}Si + ^{28}Si) ratios were thus obtained as a function of depth (Figure 3).

The diffusion coefficients were obtained by fitting the diffusion profiles to the error function,

$$c(x) = c_0 + \frac{c_1 - c_0}{2}\left(\mathrm{erf}\frac{h - x}{\sqrt{4D'_{\mathrm{Si}}\,t}} + \mathrm{erf}\frac{h + x}{\sqrt{4D'_{\mathrm{Si}}\,t}}\right) \quad (1)$$

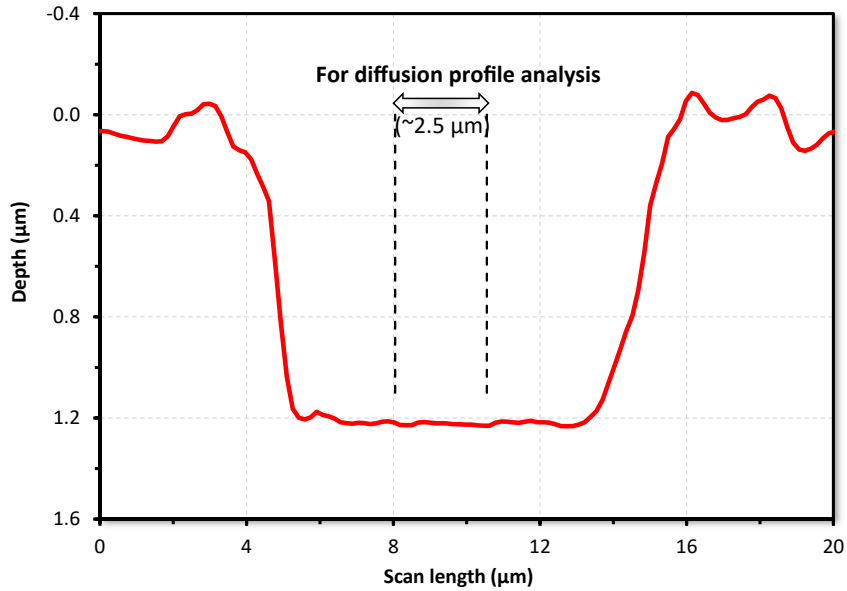

Figure 2. An example of secondary ion mass spectroscopy crater (1753). ^{29}Si and ^{28}Si intensity data from the center region of the crater with about 2.5 × 2.5 μm^2 area were used for diffusion profile analysis.

where $c(x)$ is the ^{29}Si/(^{29}Si + ^{28}Si) ratio at depth x, c_0 and c_1 are the initial ^{29}Si/(^{29}Si + ^{28}Si) ratios in the substrate and thin film, respectively, h is the position of the boundary between the thin film and substrate from the surface, t is the annealing time, and D'_{Si} is the apparent Si diffusion coefficient.

2.4. Topography Effect

The high-temperature annealing increases the sample surface roughness due to the crystallization of the thin films. The rough surfaces would broaden the diffusion profiles, causing overestimating the diffusion profiles

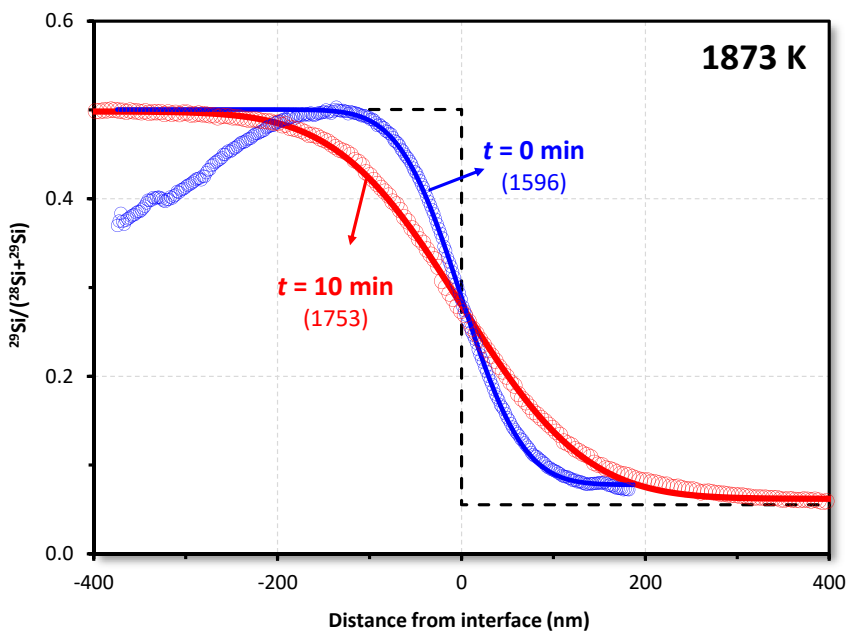

Figure 3. Examples of diffusion profiles obtained in run 1596 and 1753 at 1873 K with annealing durations of 0 (0-time run) and 10 min, respectively.

Table 1
A List of Run Conditions, C_{H2O} in the Samples Before and After Diffusion, Topography (σ, One Standard Deviation of the Topography) at the Bottom of Secondary Ion Mass Spectroscopy Craters, and Si Diffusion Coefficients

Run. No.	T (K)	t (min)	Axis	C_{H2O} (wt.ppm)[b]	C_{H2O} (wt.ppm)[c]	C_{H2O} (wt.ppm)[d]	σ (nm)	D_{Si} (m^2/s)
1695	1873	600	[100]	<10 (10)	<10 (10)	<30	52 (13)	$8.3\ (3.1) \times 10^{-19}$
1753-1	1873	10	[100]	553 (82)	520 (77)		13 (5)	$8.7\ (0.9) \times 10^{-18}$
1753-2	1873	10	[100]	553 (82)	520 (77)		34 (16)	$1.9\ (0.1) \times 10^{-17}$
1514	1873	100	[100]	291 (34)	274 (32)	315 (9)	26 (28)	$9.4\ (0.9) \times 10^{-18}$
1814-61	1673	30	[100]	1,982 (237)	1,864 (223)		22 (5)	$4.3\ (0.4) \times 10^{-18}$
1814-62	1673	30	[100]	1,982 (237)	1,864 (223)		16 (6)	$1.5\ (0.2) \times 10^{-18}$
1886	1873	600	[010]	44 (9)	50 (10)	<30	50 (14)	$3.0\ (0.3) \times 10^{-18}$
1890	1873	600	[010]	23 (3)	26 (3)	<30	41 (17)	$1.1\ (1.5) \times 10^{-18}$
1742-1	1873	15	[010]	1,136 (159)	1,282 (180)		33 (26)	$1.0\ (0.1) \times 10^{-17}$
1742-3	1873	15	[010]	1,136 (159)	1,282 (180)		39 (1)	$2.6\ (1.1) \times 10^{-17}$
1777-1	1873	20	[010]	2,634 (378)	2,973 (427)	1,710 (234)	25 (6)	$5.1\ (1.0) \times 10^{-17}$
1777-2	1873	20	[010]	2,634 (378)	2,973 (427)	1,710 (234)	57 (10)	$1.8\ (0.2) \times 10^{-17}$
1801	1873	30	[010]	2,581 (302)	2,913 (341)		7 (1)	$7.7\ (0.5) \times 10^{-17}$
1827-1	1773	20	[010]	1,802 (227)	2,034 (256)		13 (2)	$4.3\ (0.1) \times 10^{-17}$
1827-2	1773	20	[010]	1,802 (227)	2,034 (256)		14 (3)	$3.8\ (0.1) \times 10^{-17}$
1826	1773	60	[010]	5,028 (650)	5,675 (734)	6,591 (127)	9 (1)	$3.6\ (0.3) \times 10^{-17}$
1906	1673	600	[010]	2,197 (318)	2,480 (359)		35 (22)	$8.9\ (1.0) \times 10^{-18}$
1765-2	1873	15	[001]	2,541 (322)	4,032 (511)	2,573 (76)	16 (8)	$3.6\ (0.2) \times 10^{-17}$
1765-3	1873	15	[001]	2,541 (322)	4,032 (511)	2,573 (76)	16 (5)	$3.2\ (0.2) \times 10^{-17}$
1757	1873	10	[001]	2,460 (573)	3,903 (908)		51 (17)	$8.7\ (0.6) \times 10^{-17}$
1773-1	1773[a]	15	[001]	1,583 (245)	2,512 (388)		19 (8)	$1.0\ (0.2) \times 10^{-17}$
1773-2	1773[a]	15	[001]	1,583 (245)	2,512 (388)		32 (10)	$2.4\ (0.1) \times 10^{-17}$
1814-81	1673	30	[001]	1,562 (196)	2,478 (312)	1,710 (234)	3 (1)	$1.3\ (0.1) \times 10^{-18}$
1802-1	1673	60	[001]	5,301 (764)	8,411 (1,212)	6,591 (127)	28 (12)	$2.6\ (0.1) \times 10^{-17}$
1802-2	1673	60	[001]	5,301 (764)	8,411 (1,212)	6,591 (127)	28 (10)	$2.4\ (0.1) \times 10^{-17}$
1817	1573	150	[001]	2,448 (443)	3,884 (688)		35 (8)	$1.6\ (0.2) \times 10^{-18}$

[a]Temperature estimated from the power-temperature relationship from other runs. [b]C_{H2O} based on unpolarized Fourier transformation infrared spectroscopy analysis with infrared light parallel to [100], [010], or [001] following the axes for Si diffusion. [c]C_{H2O} after orientation correction using the C_{H2O} with **E**//[100], **E**//[010], and **E**//[001] polarizations reported in Jacobsen et al. (2005). [d]C_{H2O} before diffusion annealing (with random orientation).

as described previously (e.g., Dohmen, Becker, et al., 2002; Fei et al., 2012, 2013, 2014). The sample surface in this study also became very rough even by the protection using diamond single crystals. It was therefore frequently difficult to find an area on the sample surface with topography of less than 100 nm in an $80 \times 80\ \mu m^2$ area, which was the typical crater size in previous studies using SIMS Cameca-3f or Cameca-6f (e.g., Costa & Chakraborty, 2008; Fei et al., 2012, 2013; Shimojuku et al., 2004, 2009, 2010). Areas with less than 100 nm topography were generally limited to $20 \times 20\ \mu m^2$. Such small crater sizes with high mass resolutions were achieved by using a NanoSIMS. By reducing the crater size to $10 \times 10\ \mu m^2$, the surface topography within the craters was suppressed to less than 60 nm, and mostly less than 40 nm, as listed in Table 1.

Additionally, we performed zero-time runs, in which the samples were heated to the target temperature and then quenched immediately. The nominal diffusion profiles in the samples from zero-time runs were analyzed by NanoSIMS as well (Figure 3). The nominal diffusion lengths (L) in these runs were found to be a linear function of surface topography (σ), which agrees well with that determined by Fei et al. (2012) (Figure 4). The D'_{Si} in the real diffusion experiments obtained from Equation 1 was thus corrected using the following linear relationship (Ganguly et al., 1988),

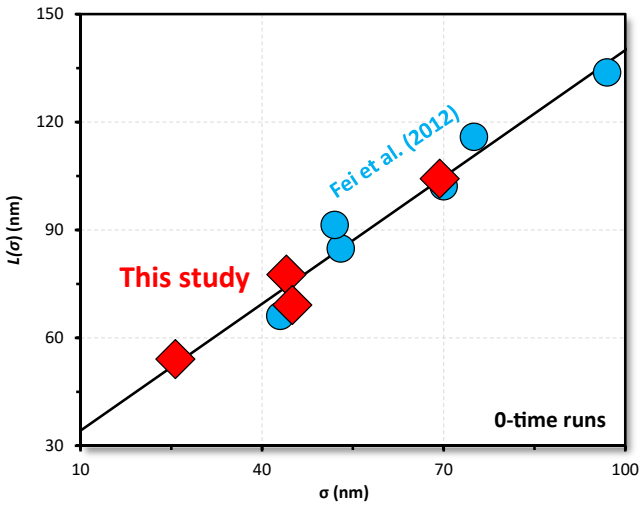

Figure 4. Linear relationship between nominal diffusion length (L) in zero-time runs and the standard deviation of surface topography (σ) in the secondary ion mass spectroscopy crater. The data points obtained in this study using Cameca NanoSIMS agree well with those obtained in Fei et al. (2012) using Cameca IMS-6f.

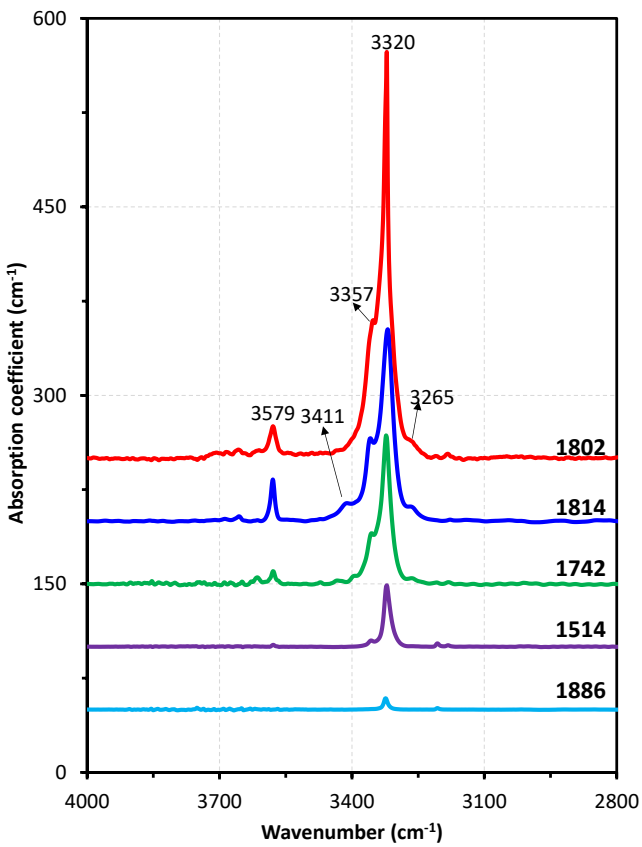

Figure 5. Examples of Fourier transformation infrared spectroscopy (FTIR) spectra in the recovered samples after baseline correction and thickness normalization to 1 cm. The spectra agree well with typical FTIR spectra of wadsleyite with strong absorptions at 3,320 and 3,357 cm^{-1}, and relatively weak absorptions at 3,579 and 3,265 cm^{-1}.

$$4D_{Si}t = 4D'_{Si}\,t - L^2(\sigma) \quad (2)$$

where D_{Si} is the Si diffusion coefficient after the correction. The Equation 2 covers the corrections of the SIMS convolution effect (depth resolution of SIMS), diffusion during heating up to the target temperature, and the relatively small contribution by the surface topography.

2.5. FT-IR Spectroscopy

The H_2O content in each recovered sample was determined by unpolarized Fourier transformation infrared spectroscopy (FTIR) using a Bruker IFS 120 high-resolution spectrometer coupled with a Bruker IR microscope. One or two hundred scans were accumulated for each spectrum at a resolution of 2 cm^{-1} with infrared light parallel to [100], [010], or [001] following the polished planes for diffusion experiments (Table 1). Examples of the spectra are given in Figure 5.

The H_2O contents in the samples were calculated using the Beer-Lambert law,

$$C_{H2O} = 10^6 \times \int \frac{3H(\upsilon)M_{H2O}}{\varepsilon\tau\rho}d\upsilon \quad (3)$$

where C_{H2O} is the H_2O content in wt. ppm, $H(\upsilon)$ is the infrared absorption at wavenumber υ, M_{H2O} is the molar weight of H_2O (18.02 g/mol), ε is the absorption coefficient (ε = 69,000 ± 7,000 L mol^{-1} cm^{-2} for Fe-free wadsleyite determined by Bolfan-Casanova et al., 2018), τ is the sample thickness, and ρ is the density ($\rho \approx$ 3,500 g L^{-1} under hydrous conditions [Jacobsen et al., 2005]). After background subtraction, the integration was performed in the range of 3,000–4,000 cm^{-1}. It is noted that the infrared spectra of wadsleyite is anisotropic (Jacobsen et al., 2005), thus, C_{H2O} based on unpolarized FTIR spectra obtained on the particular planes may cause biases. Therefore, the C_{H2O} values were corrected using the ratio of C_{H2O} with **E**//[100], **E**//[100], and **E**//[100] polarizations given in Jacobsen et al. (2005) in addition to those without orientation correction as shown in Table 1.

Because the sample surrounding (gold) cannot absorb any H_2O, the C_{H2O} in the samples did not vary significantly, that is, within a factor of 1.5 (Table 1), which is acceptable in log scale by considering the experimental uncertainty (Figure 6). Additionally, proton diffusion in wadsleyite is extremely fast ($10^{-9.5}$–$10^{-10.5}$ m^2/s at 1573–1873 K) (Sun et al., 2018), the H_2O in wadsleyite should reach equilibrium within 1 min. Therefore, the C_{H2O} measured in the recovered samples should represent the C_{H2O} condition during diffusion annealing.

3. Experimental Results

The experimental results show that D_{Si} increases systematically by about two orders of magnitude with increasing C_{H2O} from ~10 to 5,300 wt. ppm (Figure 6). On the other hand, D_{Si} increases by about 1.5 orders of magnitude with increasing temperature from 1573 to 1873 K (Figure 7). The D_{Si} show indistinguishable values in the [100], [010], and [001] directions, indicating no detectable anisotropy of Si diffusion in wadsleyite (Figures 6 and 7).

The data points are fitted to the Arrhenius equation with the H_2O content factor,

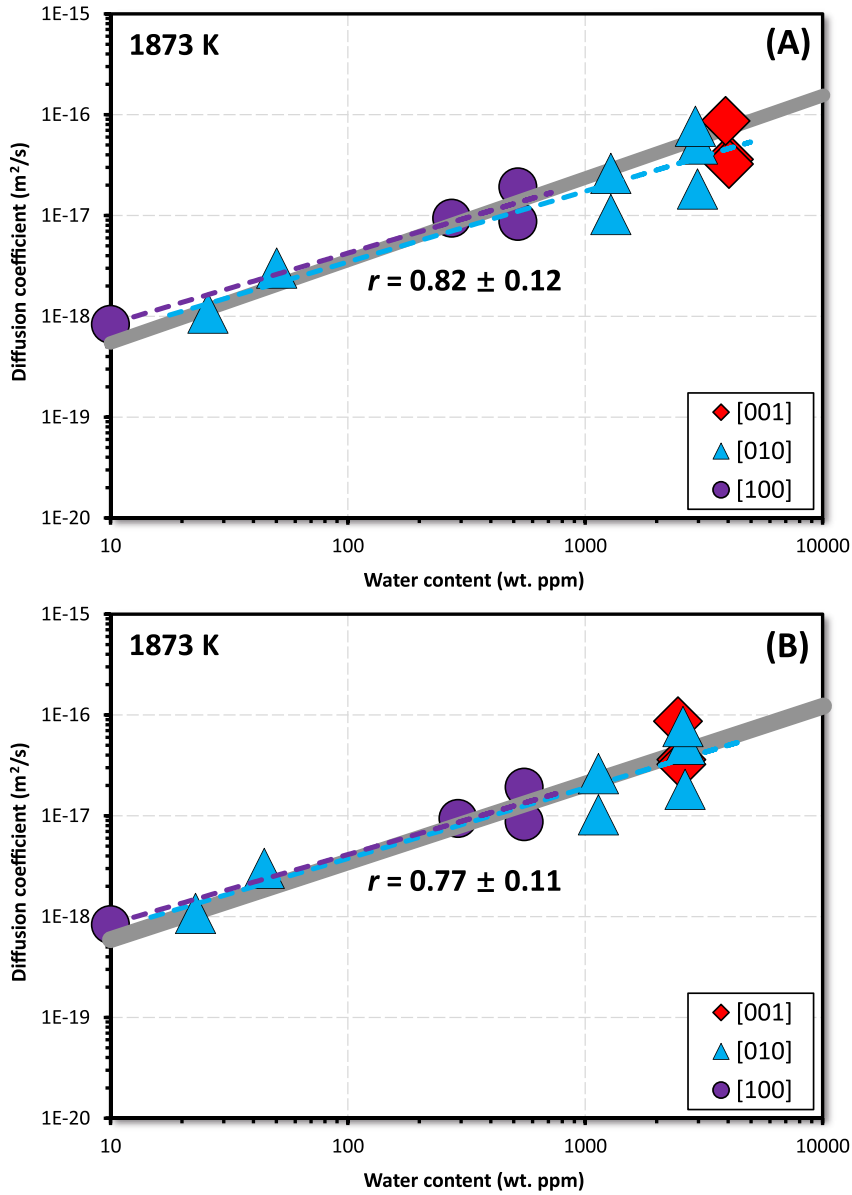

Figure 6. H_2O content dependence of Si diffusion coefficient in wadsleyite at 1873 K along [100], [010], and [001] directions. (a). Based on C_{H2O} without orientation correction. (b). Based on C_{H2O} with orientation correction. The dash lines are fitting curves of [010] and [001] data points. The thick gray line is fitting of all the data points.

$$D_{Si} = D_0(C_{H2O})^r \exp\left(-\frac{\Delta H}{RT}\right) \quad (4)$$

where D_0 is the pre-exponential factor, r is the C_{H2O} exponent, ΔH is the activation enthalpy, R is the gas constant, and T is the absolute temperature. The least squares fitting yields $D_0 = 10^{-11.5 \pm 1.1}$ m^2/s, $r = 0.8 \pm 0.1$, and $\Delta H = 270 \pm 40$ kJ/mol, by assuming r independent from T. The fitting of r based on C_{H2O} without and with orientation correction do not show meaningful difference ($r = 0.82 \pm 0.12$ and 0.77 ± 0.11, respectively, as shown in Figure 6).

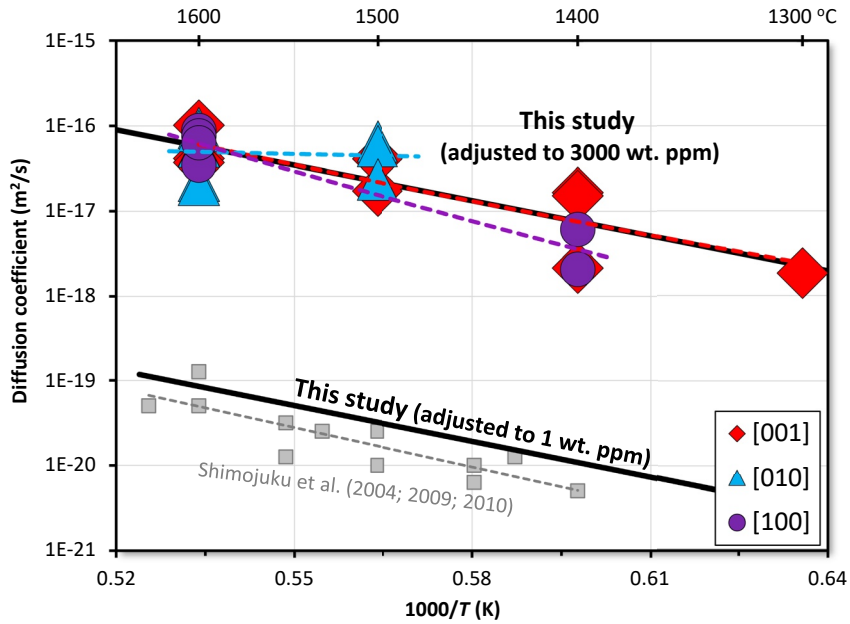

Figure 7. Temperature dependence of Si diffusion coefficient in wadsleyite along [100], [010], and [001] directions. The data points from this study are adjusted to a H_2O content of 3,000 and 3,001 wt. ppm using the C_{H2O}-exponent of $r = 0.8$. The data points from Shimojuku et al. (2004, 2009; 2010) were obtained from polycrystalline samples with H_2O content of 10–140 wt. ppm. The dash lines are fitting curves of [100], [010], and [001] data points, respectively. The black line is fitting of all the data points.

4. Discussions

4.1. H_2O Content and Temperature Dependences of D_{Si}

As mentioned in the introduction, the C_{H2O} exponent for Si diffusion in wadsleyite was not quantitatively determined previously. In the present study, the H_2O enhancement of Si diffusion in wadsleyite is quantitatively determined with a C_{H2O} exponent of $r = 0.8 \pm 0.1$ (Figure 6). It indicates that H_2O incorporation significantly enhances Si diffusion in wadsleyite, which is a strong contrast to the Si diffusion in its low-pressure polymorph, olivine ($r = 0.32 \pm 0.07$ [Fei et al., 2013]), and contrast to the Mg diffusion (D_{Mg}) in wadsleyite ($r = 0.3 \pm 0.1$ [Zhang et al., 2021]).

The temperature dependence of D_{Si} determined in this study is comparable with those reported previously (Shimojuku et al., 2004, 2009; 2010). However, the absolute values of D_{Si} in this study are higher (Figure 7), that is, D_{Si} from this study after C_{H2O} adjusting to 1 wt. ppm using the C_{H2O} exponent of 0.8 is comparable with those reported in Shimojuku et al. (2004, 2009, 2010) with 10–140 wt. ppm (Figure 7). This discrepancy could be caused by multiple reasons, (a) polycrystalline samples were used in Shimojuku et al. (2004, 2009, 2010), which may potentially enlarge the uncertainties because $\sqrt{4D_{Si}t}$ and c_0 in Equation 1 are less constrained in fitting due to the contributions of grain-boundary diffusion (e.g., Figure 4 in Shimojuku et al., 2010); (b) the surface topography in Shimojuku et al. (2004, 2009, 2010) are 40–300 nm, which is comparable with their reported $\sqrt{4D_{Si}t}$. Namely, the lattice diffusion is partially hidden by topography; (c) the actual Si activity could be systematically different although both Shimojuku et al. (2004, 2009, 2010) and this study are buffered by SiO_2; (d) the actual temperature in the cell assemblies of this study and Shimojuku et al. (2004, 2009, 2010) could be systematically different although both are self-consistent. However, all of those causes should not affect the C_{H2O} exponent for D_{Si} determined in this study.

4.2. Defect Chemistry Model

Comparison of the C_{H2O} exponent for D_{Si} in wadsleyite with its lower-pressure polymorph, olivine, shows that, H_2O incorporation dramatically enhances the Si diffusion in wadsleyite ($r = 0.8 \pm 0.1$ determined in this study), but only slightly in olivine ($r = 0.32 \pm 0.07$ [Fei et al., 2013]). In contrast, the D_{Mg} in olivine is significantly enhanced

Table 2
f_{H2O} Exponents for Defect Concentrations Under Various Charge Neutrality Conditions

Charge neutrality	$[Fe_{Mg}^{\bullet}]$	$[V_{Mg}'']$	$[H_{Mg}']$	$[(2H)_{Mg}^{\times}]$	$[V_{Si}'''']$	$[H_{Si}''']$	$[(2H)_{Si}'']$	$[(3H)_{Si}']$	$[(4H)_{Si}^{\times}]$
$[Fe_{Mg}^{\bullet}] = 2[V_{Mg}'']$	0	0	1/2	1	0	1/2	1	3/2	2
$[(OH)_O^{\bullet}] = 2[V_{Mg}'']$	−1/6	1/3	2/3	1	2/3	1	4/3	5/3	2
$[Fe_{Me}^{\bullet}] = [H_{Mg}']$	1/4	−1/2	1/4	1	−1	−1/4	1/2	5/4	2
$[(OH)_O^{\bullet}] = [H_{Mg}']$	0	0	1/2	1	0	1/2	1	3/2	2
$[(OH)_O^{\bullet}] = 4[V_{Si}'''']$	−1/10	1/5	3/5	1	2/5	4/5	6/5	8/5	2
$[(OH)_O^{\bullet}] = 3[H_{Si}''']$	0	0	1/2	1	0	1/2	1	3/2	2
$[(OH)_O^{\bullet}] = 2[(2H)_{Si}'']$	1/6	−1/3	1/3	1	−2/3	0	2/3	4/3	2
$[(OH)_O^{\bullet}] = [(3H)_{Si}']$	1/2	−1	0	1	−2	−1	0	1	2

Note. The C_{H2O} is proportional to f_{H2O} if protons are primarily hold by the defects which has an f_{H2O} exponent of 1. The exponent values are calculated following Kohlstedt (2006).

by H_2O incorporation ($r = 1.2 \pm 0.2$ for D_{Mg} [Fei et al., 2018], $r = 0.9 \pm 0.3$ for $D_{Fe\text{-}Mg}$ [Fe-Mg interdiffusion, Hier-Majumder et al., 2005]), whereas that in wadsleyite has very small C_{H2O} dependence ($r = 0.3 \pm 0.1$ for $D_{Fe\text{-}Mg}$ [Zhang et al., 2021]) (Table 2). For the higher-pressure form, ringwoodite, If the C_{H2O} exponent for D_{Si} in ringwoodite is equal to that of the dislocation mobility ($r = 1.1 \pm 0.1$) (Fei et al., 2017), the C_{H2O} exponent for D_{Si} of wadsleyite is slightly smaller than that of ringwoodite. On the other hand, the $D_{Fe\text{-}Mg}$ in ringwoodite has an C_{H2O} exponent of 0.25 ± 0.03 (Zhang et al., 2019), which is comparable with that in wadsleyite (Zhang et al., 2021) and much smaller than that in olivine (Fei et al., 2018). Below we discuss the defect chemistry of the three polymorphs individually to interpret the different C_{H2O} exponents for D_{Si} and D_{Mg}.

The Si and Mg diffusion occur by migration of Si and Mg ions from regular sites to neighboring vacant sites by the vacancy diffusion mechanism. Therefore, D_{Si} and D_{Mg} should be proportional to the concentrations of the corresponding rate-limiting defects, that is, $D_{Si} \propto [V_{Si}]$, $D_{Mg} \propto [V_{Mg}]$ (here V_{Si} and V_{Mg}, respectively, are defects related to Si and Mg that are hydrated or unhydrated). Thus, the C_{H2O} exponents for D_{Si} and D_{Mg} can be understood by the C_{H2O} exponents (and H_2O fugacity [f_{H2O}] exponents) for defect concentrations under hydrous conditions.

Protons are incorporated into wadsleyite primarily by substituting the Mg sites, where one Mg ion is replaced by two protons (e.g., Demouchy et al., 2005; Druzhbin et al., 2021; Fei & Katsura, 2021; Litasov et al., 2011; Purevjav et al., 2016), leading to much higher defect concentrations on the Mg sites than the Si sites. The primary hydration reaction is,

$$Mg_{Mg}^{\times} + 2O_O^{\times} + H_2O = \left\{ V_{Mg}'' - 2(OH)_O^{\bullet} \right\}^{\times} + MgO \quad (5)$$

where the defect association $\{V_{Mg}''-2(OH)_O^{\bullet}\}^{\times}$ is equivalent with $(2H)_{Mg}^{\times}$. The dominance of this hydration reaction leads to $C_{H2O} \propto f_{H2O}$ (Kohlstedt, 2006).

A certain fraction of $(2H)_{Mg}^{\times}$ may dissociate to $(OH)_O^{\bullet}$, V_{Mg}'', and H_{Mg}' (e.g., Kohlstedt, 2006; Kohlstedt & Hansen, 2015) as,

$$(2H)_{Mg}^{\times} \equiv \left\{ V_{Mg}'' - 2(OH)_O^{\bullet} \right\}^{\times} = H_{Mg}' + (OH)_O^{\bullet} \quad (6)$$

$$(H)_{Mg}' \equiv \left\{ V_{Mg}'' - (OH)_O^{\bullet} \right\}' = V_{Mg}'' + (OH)_O^{\bullet} \quad (7)$$

Under these circumstances, the charge neutrality conditions in Fe-free hydrous wadsleyite is expected to be maintained by $[(OH)_O^{\bullet}] = 2[V_{Mg}'']$ or $[(OH)_O^{\bullet}] = [H_{Mg}']$ (e.g., Fei & Katsura, 2016; Kohlstedt, 2006). With each charge neutrality conditions, the concentrations of different defects increase or decrease by increasing f_{H2O} with different exponents (Table 2).

The current C_{H2O} exponent of $r = 0.8 \pm 0.1$ for D_{Si} in Fe-free wadsleyite suggests that Si diffusion is controlled by either $(2H)_{Si}''$ with the charge neutrality condition of $[(OH)_O^{\bullet}] = [H_{Mg}']$ ($[(2H)_{Si}''] \propto C_{H2O}^{1}$ shown in Table 2) or by V_{Si}'''' or H_{Si}''' with the charge neutrality condition of $[(OH)_O^{\bullet}] = 2[V_{Mg}'']$ ($[V_{Si}''''] \propto C_{H2O}^{2/3}$ $[H_{Si}'''] \propto C_{H2O}^{1}$, Table 2). In other words $(3H)_{Si}'$ and $(4H)_{Si}^{\times}$ are unlikely to dominate Si diffusion in Fe-free wadsleyite because they will result in much larger C_{H2O} exponents (≥3/2, Table 2).

In Fe-bearing wadsleyite, Nishihara, Shinmei, Karato (2008) suggested a charge neutrality condition of $[Fe_{Mg}^{\bullet}] = [H_{Mg}']$. This condition leads to the C_{H2O} exponents of 1/4 for both $[H_{Mg}']$ and $[Fe_{Mg}^{\bullet}]$, explaining the H_2O exponent of $r = 0.3 \pm 0.1$ for $D_{Fe\text{-}Mg}$ reported by Zhang et al. (2021). If V_{Si}'''' or H_{Si}''' dominated Si diffusion, D_{Si} would have a negative C_{H2O} dependence (Table 2), which is against the water-weakening of Fe-bearing wadsleyite (Hustoft et al., 2013). Thus, V_{Si}'''' and H_{Si}''' are excluded as the dominant species for Si diffusion in Fe-bearing wadsleyite. Therefore, if we assume the same Si diffusion mechanism in Fe-bearing and Fe-free wadsleyite, D_{Si} is most likely controlled by migration of $(2H)_{Si}''$.

Fe-bearing hydrous ringwoodite has a C_{H2O} exponent of $r = 0.25 \pm 0.03$ for $D_{Fe\text{-}Mg}$ (Zhang et al., 2019), indicating the charge neutrality condition of $[Fe_{Mg}^{\bullet}] = [H_{Mg}']$. Therefore, the $r = 1.1 \pm 0.1$ for D_{Si} inferred from dislocation annihilation rate in Fe-bearing ringwoodite (Fei et al., 2017) suggests a $(3H)_{Si}'$-controlled Si diffusion mechanism because $[(3H)_{Si}'] \propto C_{H2O}^{5/4}$. The V_{Si}'''', H_{Si}''', $(2H)_{Si}''$, and $(4H)_{Si}^{\times}$ are all unlikely because of their much smaller ($r \leq 1/2$) or larger ($r = 2$) C_{H2O} exponents (Table 2).

In olivine, proton incorporation occurs by substituting the Si sites with the reaction $Si_{Si}^{\times} + 4O_O^{\times} + 2H_2O = V_{Si}''''$ $+ 4(OH)_O^{\bullet} + SiO_2$ (e.g., Fei & Katsura, 2020b). Therefore, the charge neutrality condition could be maintained by V_{Si}'''' and $(OH)_O^{\bullet}$ (Table 2). The $r = 0.32 \pm 0.07$ for D_{Si} and $r = 0.9$–1.2 for D_{Mg} in olivine (Fei et al., 2013, 2018; Hier-Majumder et al., 2005) suggest that Si and Mg diffusion are most likely controlled by V_{Si}'''' and $(2H)_{Mg}^{\times}$, respectively, under the charge neutrality condition of $[(OH)_O^{\bullet}] = 4[V_{Si}'''']$ because of $[V_{Si}''''] \propto C_{H2O}^{2/5}$ and $[(2H)_{Mg}^{\times}] \propto C_{H2O}^{1}$ (Table 2) by assuming $C_{H2O} \propto f_{H2O}$ (Kohlstedt et al., 1996; Zhao et al., 2004). However, depending on the dominant defects for holding protons, C_{H2O} and f_{H2O} may not follow a linear relationship (Otsuka & Karato, 2011), thus, the C_{H2O} exponents for D_{Si} and D_{Mg} may not equal the f_{H2O} exponents for $[V_{Si}]$ and $[V_{Mg}]$. For example, if protons are hold primarily by $(2H)_{Si}''$ and the charge neutrality condition is $[(OH)_O^{\bullet}] = 4[V_{Si}'''']$, we have $C_{H2O} \propto [(2H)_{Si}''] \propto f_{H2O}^{6/5}$, thus, $D_{Si} \propto [V_{Si}''''] \propto f_{H2O}^{2/5} \propto C_{H2O}^{1/3}$ (Table 2), which also agree with the experimental results. To better constrain the Si diffusion mechanism in hydrous olivine, precise f_{H2O} and C_{H2O} relationship is required.

4.3. Isotropic Si Diffusivity in Mantle Minerals

As shown in Figures 6 and 7, the D_{Si} in wadsleyite is found to be isotropic under both H_2O-poor and H_2O-rich conditions. The least squares fitting of data points for each crystallographic axis suggest an apparent maximum anisotropy factor of about three at 1500–1600°C (Figure 7), but this apparent value is caused by the scattering of [010] data points. The actual anisotropy is expected to be much smaller than three. The nearly isotropic Si diffusion is also the case of other mantle minerals including olivine (Costa & Chakraborty, 2008), bridgmanite (Xu et al., 2011), quartz, and feldspar (Cherniak, 2003). Although small anisotropy is reported in stishovite (Shatskiy et al., 2010), its magnitude of anisotropy is within experimental uncertainty as well. In contrast, the Mg diffusion in olivine is found to be anisotropic (Chakraborty et al., 1994).

It is known that self-diffusion in a crystal occurs by hopping of the diffusing species driven by thermal vibrations. The probabilities of successful hops along various crystallographic directions, which are related to the frequencies and activation barriers of the thermal vibrations, control the diffusion anisotropy. In the case of Mg diffusion, the activation barrier is related to the distances between two Mg ions, therefore, the diffusion anisotropy is correlated to the distances (e.g., Brodholt, 1997). In the case of Si, the activation barrier is primarily controlled by the local environment, that is, limited by the escape of a Si ion from the closely packed SiO_4 tetrahedron regardless of diffusion direction. Hence, the diffusion coefficient is nearly isotropic.

4.4. H_2O-Induced Viscosity Reduction in the Mantle Transition Zone

Because the viscosity of silicate minerals is considered to be inversely proportional to the diffusion coefficient of Si, the H_2O enhancement of D_{Si} will induce the reduction of viscosity. Using the C_{H2O} exponent of 0.8, the

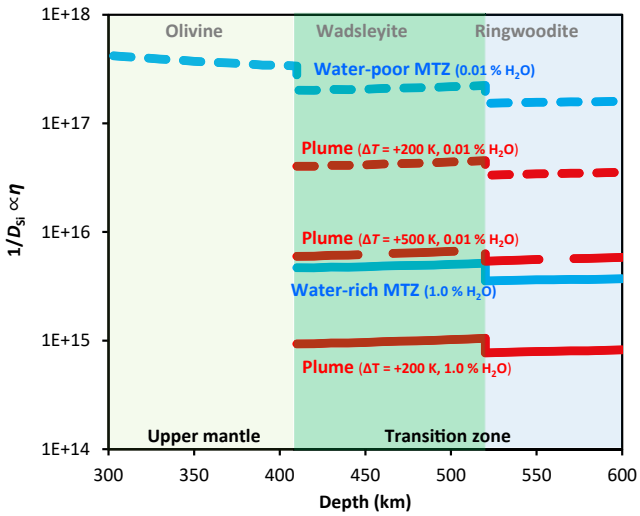

Figure 8. Relative viscosity ($\eta \propto 1/D_{Si}$) in the transition zone and plumes at various H_2O content and temperature conditions. The temperature in the plumes is assumed to be 200–500 K higher (ΔT) than normal geotherm (Katsura et al., 2010). The pressure dependence of D_{Si} is assumed to be the same as olivine (Fei et al., 2012). MTZ: mantle transition zone.

viscosity of H_2O-rich wadsleyite (C_{H2O} = ~1.0 wt.%, H_2O-saturated wadsleyite at mantle transition zone temperature [Fei & Katsura, 2021]) is by 1.6 orders of magnitude lower than H_2O-poor wadsleyite (C_{H2O} = ~0.01 wt.%) (Figure 8). On the other hand, although the C_{H2O} exponent for D_{Si} in ringwoodite is unknown, it can be estimated to be $r \approx 1.1$ based on the H_2O dependence of dislocation-annihilation rate in ringwoodite (Fei et al., 2017). Therefore, the H_2O incorporation dramatically reduces the viscosity of both wadsleyite and ringwoodite, the dominant minerals in the upper (410–520 km depth) and lower (520–660 km depth) part of mantle transition zone, respectively (Figure 8).

4.5. Evolution of Plumes in the Mantle Transition Zone

Seismic observations of the 60 plumes (e.g., Zhao, 2007) indicate that the mantle transition zone induces enigmatic evolutions of the plumes when crossing the 410–660 km layer. Some plumes such as Iceland, Hainan, and Galapagos are accelerated and narrowed in the mantle transition zone, whereas some others such as Hawaii, East Australia are broadened or curved. The cause of such enigmatic evolutions is unknown.

The plume shape is controlled by the viscosity contrast between the upwelling flow and materials in the surrounding mantle (Condie, 2016). When the plume has a lower viscosity than the surrounding mantle, it will appear like a mushroom with a broad head and may be curved by the horizontal flow driven by plate tectonics. On the other hand, when the plume has a higher viscosity than the surroundings, it will rise straightly with its original thickness or could be slightly narrowed because of cooling of the plume edges by the surroundings. Therefore, the viscosity contrast of wadsleyite (and ringwoodite) between the plumes and the surrounding mantle may provide an answer for the origin of the mystical evolution of plumes in the mantle transition zone.

Combining the H_2O and temperature effects on Si diffusion coefficient in wadsleyite determined in this study, the viscosity contrast between the plume and surrounding mantle in the transition zone can be evaluated with various temperature and H_2O content conditions. As shown in Figure 8, if the plume has a low H_2O content (C_{H2O} = 0.01 wt.%) and relatively low temperature [ΔT = +200 K, that is, 200 K higher than normal geotherm (Katsura et al., 2010), the plume viscosity will be higher than a H_2O-rich mantle transition zone by about one order of magnitude. In contrast, when the plume has either high temperature (ΔT = +500 K) or high H_2O content (C_{H2O} = 1.0 wt.%), the viscosity will be significantly reduced and become comparable or even lower than a H_2O-rich transition zone. However, if the mantle transition zone is H_2O-poor, the plume viscosity will be always lower than the surrounding mantle because $\Delta T > 0$ (Figure 8).

Most of the plumes are originated from the deep lower mantle (Condie, 2016; Zhao, 2007). Therefore, they should be H_2O-poor because of the dry lower mantle (Hirschmann, 2006; Liu et al., 2021). On the other hand, the mantle transition zone is demonstrated to be H_2O-rich at least locally (Kelbert et al., 2009; Pearson et al., 2014) or even globally (Fei et al., 2017). Thus, the plumes with a relatively low-temperature (still higher than the transition zone, e.g., ΔT = +200 K in Figure 8) are expected to be accelerated and narrowed because of it has higher viscosity than the transition zone. On the other hand, the plumes that are broadened or curved in the mantle transition zone are expected to have either relatively high temperature (e.g., $\Delta T \geq$ +500 K) or locally dry surrounding mantle.

In case of either narrowed or broadened in the mantle transition zone, eventually, the upwelling flows will reach the 410-km depth boundary between the transition zone and upper mantle. Because the upper mantle has low H_2O content (~100 wt. ppm), the plumes will have lower viscosity than the surrounding mantle and therefore been broadened just beneath 410-km depth. It explains the inverted-triangle-shape of the narrowed plumes such as Iceland, Galapagos, Hainan, and San Felix near the 410-km depth boundary (Zhao, 2007).

Data Availability Statement

The SIMS and FTIR data for this paper are given in Zenodo (https://doi.org/10.5281/zenodo.6265716).

Acknowledgments
We appreciate H. Fischer for the preparation of high-pressure cell assembly, R. Njul for sample polishing, and Dr. Jianchao Zhang for assistance in SIMS analysis. We also appreciate two anonymous reviewers for helpful comments. This work is financially supported by the Deutsche Forschungsgemeinschaft to T. Katsura (KA3434/7-1, KA3434/8-1) and the annual budget of Bayerisches Geoinstitut to H. Fei. Open access funding enabled and organized by Projekt DEAL.

References

Bolfan-Casanova, N., Schiavi, F., Novella, D., Bureau, H., Raepsaet, C., Khodja, H., & Demouchy, S. (2018). Examination of water quantification and incorporation in transition zone minerals: Wadsleyite, ringwoodite, and phase D using ERDA (elastic recoil detection analysis). *Frontiers of Earth Science*, *6*, 75. https://doi.org/10.3389/feart.2018.00075

Brodholt, J. (1997). Ab initio calculations on point defects in forsterite (Mg_2SiO_4) and implications for diffusion and creep. *American Mineralogist*, *82*, 1049–1053. https://doi.org/10.2138/am-1997-11-1201

Chakraborty, S., Farver, J. R., Yund, R. A., & Rubie, D. C. (1994). Mg trace diffusion in synthetic forsterite and San Carlos olivine as a function of P, T, and f_{O2}. *Physics and Chemistry of Minerals*, *21*, 489–500. https://doi.org/10.1007/bf00203923

Cherniak, D. J. (2003). Silicon self-diffusion in single-crystal natural quartz and feldspar. *Earth and Planetary Science Letters*, *214*, 655–668. https://doi.org/10.1016/s0012-821x(03)00394-7

Condie, K. C. (2016). The mantle. In K. C. Condie (Ed.), *Earth as an evolving planetary system* (pp. 89–133). Academic Press. https://doi.org/10.1016/b978-0-12-803689-1.00004-3

Costa, F., & Chakraborty, S. (2008). The effect of water on Si and O diffusion rates in olivine and implications for transport properties and processes in the upper mantle. *Physics of the Earth and Planetary Interiors*, *166*, 11–29. https://doi.org/10.1016/j.pepi.2007.10.006

Dai, L., & Karato, S. I. (2009). Electrical conductivity of wadsleyite at high tempeatures and high pressures. *Earth and Planetary Science Letters*, *287*, 277–283. https://doi.org/10.1016/j.epsl.2009.08.012

Demouchy, S., Deloule, E., Frost, D. J., & Keppler, H. (2005). Pressure and temperature-dependence of water solubility in Fe-free wadsleyite. *American Mineralogist*, *90*, 1084–1091. https://doi.org/10.2138/am.2005.1751

Dohmen, R., Becker, H. W., Meißner, E., Etzel, T., & Chakraborty, S. (2002). Production of silicate thin films using pulsed laser deposition (PLD) and applications to studies in mineral kinetics. *European Journal of Mineralogy*, *14*, 1155–1168. https://doi.org/10.1127/0935-1221/2002/0014-1155

Dohmen, R., Chakraborty, S., & Becker, H. W. (2002). Si and O diffusion in olivine and implications for characterizing plastic flow in the mantle. *Geophysical Research Letters*, *29*(21), 26–1. https://doi.org/10.1029/2002gl015480

Druzhbin, D., Fei, H., & Katsura, T. (2021). Independent hydrogen incorporation in wadsleyite from oxygen fugacity and non-dissociation of H_2O in the reducing mantle transition zone. *Earth and Planetary Science Letters*, *557*, 116755. https://doi.org/10.1016/j.epsl.2021.116755

Farla, R., Amulele, G., Girard, J., Miyajima, N., & Karato, S. I. (2015). High-pressure and high-temperature deformation experiments on polycrystalline wadsleyite using the rotational Drickamer apparatus. *Physics and Chemistry of Minerals*, *42*, 541–558. https://doi.org/10.1007/s00269-015-0742-0

Fei, H., Hegoda, C., Yamazaki, D., Wiedenbeck, M., Yurimoto, H., Shcheka, S., & Katsura, T. (2012). High silicon self-diffusion coefficient in dry forsterite. *Earth and Planetary Science Letters*, *345*, 95–103. https://doi.org/10.1016/j.epsl.2012.06.044

Fei, H., & Katsura, T. (2016). Si and O self-diffusion in forsterite and iron-bearing olivine from the perspective of defect chemistry. *Physics and Chemistry of Minerals*, *43*(2), 119–126. https://doi.org/10.1007/s00269-015-0779-0

Fei, H., & Katsura, T. (2020a). High water solubility of ringwoodite at mantle transition zone temperature. *Earth and Planetary Science Letters*, *531*, 115987. https://doi.org/10.1016/j.epsl.2019.115987

Fei, H., & Katsura, T. (2020b). Pressure dependence of proton incorporation and water solubility in olivine. *Journal of Geophysical Research: Solid Earth*, *125*, e2019JB018813. https://doi.org/10.1029/2019jb018813

Fei, H., & Katsura, T. (2021). Water solubility in Fe-bearing wadsleyite at mantle transition zone temperatures. *Geophysical Research Letters*, *48*, e2021GL092836. https://doi.org/10.1029/2021gl092836

Fei, H., Koizumi, S., Sakamoto, N., Hashiguchi, M., Yurimoto, H., Marquardt, K., et al. (2018). Mg lattice diffusion in iron-free olivine and implications to conductivity anomaly in the oceanic asthenosphere. *Earth and Planetary Science Letters*, *484*, 204–212. https://doi.org/10.1016/j.epsl.2017.12.020

Fei, H., Wiedenbeck, M., Yamazaki, D., & Katsura, T. (2013). Small effect of water on upper-mantle rheology based on silicon self-diffusion coefficients. *Nature*, *498*, 213–215. https://doi.org/10.1038/nature12193

Fei, H., Wiedenbeck, M., Yamazaki, D., & Katsura, T. (2014). No effect of water on oxygen self-diffusion rate in forsterite. *Journal of Geophysical Research: Solid Earth*, *119*, 7598–7606. https://doi.org/10.1002/2014jb011141

Fei, H., Yamazaki, D., Sakurai, M., Miyajima, N., Ohfuji, H., Katsura, T., & Yamamoto, T. (2017). A nearly water-saturated mantle transition zone inferred from mineral viscosity. *Science Advances*, *3*, e1603024. https://doi.org/10.1126/sciadv.1603024

Fukao, Y., Obayashi, M., Nakakuki, T., & Deep Slab Project Group (2009). Stagnant slab: A review. *Annual Review of Earth and Planetary Sciences*, *37*, 19–46. https://doi.org/10.1146/annurev.earth.36.031207.124224

Ganguly, J., Bhattacharya, R. N., & Chakraborty, S. (1988). Convolution effects in the determination of compositional profiles and diffusion coefficients by microprobe step scan. *American Mineralogist*, *73*, 901–909.

Hier-Majumder, S., Anderson, I. M., & Kohlstedt, D. L. (2005). Influence of protons on Fe-Mg interdiffusion in olivine. *Journal of Geophysical Research*, *110*, B02202. https://doi.org/10.1029/2004jb003292

Hirschmann, M. M. (2006). Water, melting, and the deep Earth H_2O cycle. *Annual Review of Earth and Planetary Sciences*, *34*, 629–653. https://doi.org/10.1146/annurev.earth.34.031405.125211

Huang, X., Xu, Y., & Karato, S. I. (2005). Water content of the mantle transition zone from the electrical conductivity of wadsleyite and ringwoodite. *Nature*, *434*, 746–749. https://doi.org/10.1038/nature03426

Hustoft, J., Amulele, G., Ando, J., Otsuka, K., Du, Z., Jing, Z., & Karato, S. I. (2013). Plastic deformation experiments to high strain on mantle transition zone minerals wadsleyite and ringwoodite in the rotational Drickamer apparatus. *Earth and Planetary Science Letters*, *361*, 7–15. https://doi.org/10.1016/j.epsl.2012.11.028

Jacobsen, S. D., Demouchy, S., Frost, D. J., Boffa-Ballaran, T. B., & Kung, J. (2005). A systematic study of OH in hydrous wadsleyite from polarized FTIR spectroscopy and single-crystal X-ray diffraction: Oxygen sites for hydrogen storage in Earth's interior. *American Mineralogist*, *90*, 61–70. https://doi.org/10.2138/am.2005.1624

Karato, S. I. (2011). Water distribution across the mantle transition zone and its implications for global material circulation. *Earth and Planetary Science Letters*, *301*, 413–423. https://doi.org/10.1016/j.epsl.2010.11.038

Katsura, T., Yoneda, A., Yamazaki, D., Yoshino, T., & Ito, E. (2010). Adiabatic temperature profile in the mantle. *Physics of the Earth and Planetary Interiors*, *183*, 212–218. https://doi.org/10.1016/j.pepi.2010.07.001

Kawazoe, T., Nishihara, Y., Ohuchi, T., Miyajima, N., Maruyama, G., Higo, Y., et al. (2016). Creep strength of ringwoodite measured at pressure-temperature conditions of the lower part of the mantle transition zone using a deformation-DIA apparatus. *Earth and Planetary Science Letters*, *454*, 10–19. https://doi.org/10.1016/j.epsl.2016.08.011

Kawazoe, T., Nishihara, Y., Ohuchi, T., Nishiyama, N., Higo, Y., Funakoshi, K., & Irifune, T. (2011). In situ stress-strain measurements in a deformation-DIA apparatus at P-T conditions of the upper part of the mantle transition zone. *American Mineralogist*, *96*, 1665–1672. https://doi.org/10.2138/am.2011.3818

Kawazoe, T., Nishiyama, N., Nishihara, Y., & Irifune, T. (2010). Deformation experiment at P–T conditions of the mantle transition zone using D-DIA apparatus. *Physics of the Earth and Planetary Interiors*, *183*(1–2), 190–195

Kawazoe, T., Ohuchi, T., Nishihara, Y., Nishiyama, N., Fujino, K., & Irifune, T. (2013). Seismic anisotropy in the mantle transition zone induced by shear deformation of wadsleyite. *Physics of the Earth and Planetary Interiors*, *216*, 91–98. https://doi.org/10.1016/j.pepi.2012.12.005

Kelbert, A., Schultz, A., & Egbert, G. (2009). Global electromagnetic induction constraints on transition-zone water content variations. *Nature*, *460*, 1003–1006. https://doi.org/10.1038/nature08257

Kohlstedt, D. L. (2006). The role of water in high-temperature rock deformation. *Reviews in mineralogy and geochemistry*, *62*, 377–396. https://doi.org/10.1515/9781501509476-020

Kohlstedt, D. L., & Hansen, L. N. (2015). Constitutive equations, rheological behavior, and viscosity of rocks. In *Treatise on geophysics* (2nd ed., pp. 441–472). https://doi.org/10.1016/B978-0-444-53802-4.00042-7

Kohlstedt, D. L., Keppler, H., & Rubie, D. C. (1996). Solubility of water in the α, β, γ phases of $(Mg, Fe)_2SiO_4$. *Contributions to Mineralogy and Petrology*, *123*, 345–357. https://doi.org/10.1007/s004100050161

Kubo, T., Shimojuku, A., & Ohtaini, E. (2004). Mg-Fe interdiffusion in wadsleyite and the diffusivity jump at the 410-km discontinuity. *Physics and Chemistry of Minerals*, *31*, 456–464. https://doi.org/10.1007/s00269-004-0412-0

Kuritani, T., Xia, Q., Kimura, J. I., Liu, J., Shimizu, K., Ushikubo, T., et al. (2019). Buoyant hydrous mantle plume from the mantle transition zone. *Scientific Reports*, *9*(1), 1–7. https://doi.org/10.1038/s41598-019-43103-y

Litasov, K. D., Shatskiy, A., Ohtani, E., & Katsura, T. (2011). Systematic study of hydrogen incorporation into Fe-free wadsleyite. *Physics and Chemistry of Minerals*, *38*, 75–84. https://doi.org/10.1007/s00269-010-0382-3

Liu, Z., Fei, H., Chen, L., McCammon, C., Wang, L., Liu, R., et al. (2021). Bridgmanite is nearly dry at the top of the lower mantle. *Earth and Planetary Science Letters*, *570*, 117088. https://doi.org/10.1016/j.epsl.2021.117088

Manthilake, M., Matsuzaki, T., Yoshino, T., Yamashita, S., Ito, E., & Katsura, T. (2009). Electrical conductivity of wadsleyite as a function of temperature and water content. *Physics of the Earth and Planetary Interiors*, *174*, 10–18. https://doi.org/10.1016/j.pepi.2008.06.001

Mullins, W. W. (1958). The effect of thermal grooving on grain boundary motion. *Acta Metallurgica*, *6*(6), 414–427. https://doi.org/10.1016/0001-6160(58)90020-8

Nishihara, Y., Shinmei, T., & Karato, S. I. (2008). Effect of chemical environment on the hydrogen-related defect chemistry in wadsleyite. *American Mineralogist*, *93*, 831–843. https://doi.org/10.2138/am.2008.2653

Nishihara, Y., Tinker, D., Kawazoe, T., Xu, Y., Jing, Z., Matsukage, K. N., & Karato, S. I. (2008). Plastic deformation of wadsleyite and olivine at high-pressure and high-temperature using a rotational Drickamer apparatus (RDA). *Physics of the Earth and Planetary Interiors*, *170*, 156–169. https://doi.org/10.1016/j.pepi.2008.03.003

Otsuka, K., & Karato, S. I. (2011). Control of the water fugacity at high pressures and temperatures: Applications to the incorporation mechanisms of water in olivine. *Physics of the Earth and Planetary Interiors*, *189*, 27–33. https://doi.org/10.1016/j.pepi.2011.09.007

Pearson, D. G., Brenker, F. E., Nestola, F., McNeill, J., Nasdala, L., Hutchison, M. T., et al. (2014). Hydrous mantle transition zone indicated by ringwoodite included within diamond. *Nature*, *507*, 221–224. https://doi.org/10.1038/nature13080

Purevjav, N., Okuchi, T., Tomioka, N., Wang, X., & Hoffmann, C. (2016). Quantitative analysis of hydrogen sites and occupancy in deep mantle hydrous wadsleyite using single crystal neutron diffraction. *Scientific Reports*, *6*, 34988. https://doi.org/10.1038/srep34988

Revenaugh, J., & Sipkin, S. A. (1994). Seismic evidence for silicate melt atop the 410-km mantle discontinuity. *Nature*, *369*, 474–476. https://doi.org/10.1038/369474a0

Ritterbex, S., Carrez, P., & Cordier, P. (2020). Deformation across the mantle transition zone: A theoretical mineral physics view. *Earth and Planetary Science Letters*, *547*, 116438. https://doi.org/10.1016/j.epsl.2020.116438

Ritterbex, S., Carrez, P., Gouriet, K., & Cordier, P. (2015). Modeling dislocation glide in Mg_2SiO_4 ringwoodite: Towards rheology under transition zone conditions. *Physics of the Earth and Planetary Interiors*, *248*, 20–29. https://doi.org/10.1016/j.pepi.2015.09.001

Schmandt, B., Jacobsen, S. D., Becker, T. W., Liu, Z., & Dueker, K. G. (2014). Dehydration melting at the top of the lower mantle. *Science*, *344*, 1265–1268. https://doi.org/10.1126/science.1253358

Shatskiy, A., Yamazaki, D., Borzdov, Y. M., Matsuzaki, T., Litasov, K. D., Cooray, T., et al. (2010). Stishovite single-crystal growth and application to silicon self-diffusion measurements. *American Mineralogist*, *95*, 135–143. https://doi.org/10.2138/am.2010.3255

Shimojuku, A., Kubo, T., Ohtani, E., Nakamura, T., & Okazaki, R. (2010). Effects of hydrogen and iron on the silicon diffusivity of wadsleyite. *Physics of the Earth and Planetary Interiors*, *183*, 175–182. https://doi.org/10.1016/j.pepi.2010.09.011

Shimojuku, A., Kubo, T., Ohtani, E., Nakamura, T., Okazaki, R., Dohmen, R., & Chakraborty, S. (2009). Si and O diffusion in $(Mg, Fe)_2SiO_4$ wadsleyite and ringwoodite and its implications for the rheology of the mantle transition zone. *Earth and Planetary Science Letters*, *284*, 103–112. https://doi.org/10.1016/j.epsl.2009.04.014

Shimojuku, A., Kubo, T., Ohtani, E., & Yurimoto, H. (2004). Silicon self-diffusion in wadsleyite: Implications for rheology of the mantle transition zone and subducting plates. *Geophysical Research Letters*, *31*, L13606. https://doi.org/10.1029/2004gl020002

Sun, W., Yoshino, T., Sakamoto, N., & Yurimoto, H. (2018). Supercritical fluid in the mantle transition zone deduced from H-D interdiffusion of wadsleyite. *Earth and Planetary Science Letters*, *484*, 309–317. https://doi.org/10.1016/j.epsl.2017.12.032

Xu, J., Yamazaki, D., Katsura, T., Wu, X., Remmert, P., Yurimoto, H., & Chakraborty, S. (2011). Silicon and magnesium diffusion in a single crystal of $MgSiO_3$ perovskite. *Journal of Geophysical Research*, *116*, 2011JB008444. https://doi.org/10.1029/2011jb008444

Zhang, B., Yoshino, T., & Zhao, C. (2019). The effect of water on Fe-Mg interdiffusion rates in ringwoodite and implications for the electrical conductivity in the mantle transition zone. *Journal of Geophysical Research: Solid Earth*, *124*, 2510–2524. https://doi.org/10.1029/2018jb016415

Zhang, B., Zhao, C., & Yoshino, T. (2021). Fe–Mg interdiffusion in wadsleyite and implications for water content of the transition zone. *Earth and Planetary Science Letters*, *554*, 116672. https://doi.org/10.1016/j.epsl.2020.116672

Zhao, D. (2007). Seismic images under 60 hotspots: Search for mantle plumes. *Gondwana Research*, *12*, 335–355. https://doi.org/10.1016/j.gr.2007.03.001

Zhao, Y. H., Ginsberg, S. B., & Kohlstedt, D. L. (2004). Solubility of hydrogen in olivine: Dependence on temperature and iron content. *Contributions to Mineralogy and Petrology*, *147*, 155–161. https://doi.org/10.1007/s00410-003-0524-4